frontiers | Frontiers in Astronomy and Space Sciences

TYPE Original Research
PUBLISHED 10 January 2023
DOI 10.3389/fspas.2022.1033546

Check for updates

OPEN ACCESS

EDITED BY
Jonathan Eastwood,
Imperial College London, United Kingdom

REVIEWED BY
Natalia Buzulukova,
University of Maryland, United States
Shiyong Huang,
Wuhan University, China
Zhonghua Yao,
Institute of Geology and Geophysics (CAS), China

*CORRESPONDENCE
S. N. F. Chepuri,
sanjay-chepuri@uiowa.edu

SPECIALTY SECTION
This article was submitted to Space Physics, a section of the journal Frontiers in Astronomy and Space Sciences

RECEIVED 31 August 2022
ACCEPTED 28 December 2022
PUBLISHED 10 January 2023

CITATION
Chepuri SNF, Jaynes AN, Turner DL, Gabrielse C, Baker DN, Mauk BH, Cohen IJ, Leonard T, Blake JB and Fennell JF (2023), A comparison of energetic particle energization observations at MMS and injections at Van Allen Probes.
Front. Astron. Space Sci. 9:1033546.
doi: 10.3389/fspas.2022.1033546

COPYRIGHT
© 2023 Chepuri, Jaynes, Turner, Gabrielse, Baker, Mauk, Cohen, Leonard, Blake and Fennell. This is an open-access article distributed under the terms of the Creative Commons Attribution License (CC BY). The use, distribution or reproduction in other forums is permitted, provided the original author(s) and the copyright owner(s) are credited and that the original publication in this journal is cited, in accordance with accepted academic practice. No use, distribution or reproduction is permitted which does not comply with these terms.

A comparison of energetic particle energization observations at MMS and injections at Van Allen Probes

S. N. F. Chepuri[1]*, A. N. Jaynes[1], D. L. Turner[2], C. Gabrielse[3], D. N. Baker[4], B. H. Mauk[2], I. J. Cohen[2], T. Leonard[4], J. B. Blake[3] and J. F. Fennell[3]

[1]Department of Physics and Astronomy, University of Iowa, Iowa City, IA, United States, [2]The Johns Hopkins University Applied Physics Laboratory, Laurel, MD, United States, [3]Space Science Applications Laboratory, El Segundo, CA, United States, [4]Laboratory of Atmospheric and Space Physics, University of Colorado Boulder, Boulder, CO, United States

In this study, we examine particle energization and injections that show energetic electron enhancements at both MMS in the magnetotail and Van Allen Probes in the inner magnetosphere. Observing injections along with a corresponding flow burst allows us to better understand injections overall. Searching for suitable events, we found that only a small number of events at MMS had corresponding injections that penetrated far enough into the inner magnetosphere to observe with Van Allen Probes. With the four suitable events we did find, we compared the energy spectra at the two spacecraft and mapped the boundary of where the injection entered the inner magnetosphere. We found that, among these injections in the inner magnetosphere, the electron flux did not increase above ~400 keV, similar to previous results, but the corresponding signatures in the tail observed increased fluxes at 600 keV or higher. There does not appear to be a comparable flux increase at Van Allen Probes and MMS for a given event. None of our injections included ion enhancements at Van Allen Probes, but one included an ion injection at geosynchronous orbit in the GOES spacecraft. All of our injections were dispersed at Van Allen Probes, and we were therefore able to map an estimate of the injection boundary. All of the injections occurred in the premidnight sector. Although we found some events where particle energizations in the tail are accompanied by inner magnetospheric injections, we do not find a statistical link between the two.

KEYWORDS

energetic particles, injections, magnetotail, MMS, Van Allen Probes, fast flows, dipolarization

1 Introduction

Injections are the earthward transport and acceleration of energetic particles and observed as an increase in the intensity of energetic particles of 10 s–100 s of keV. They were originally observed at geosynchronous orbit (6.6 R_E) (Arnoldy and Chan, 1969), but have since been found in a range of locations on the nightside of the magnetosphere with spacecraft like LANL at geosynchronous orbit (GEO) and THEMIS downtail in the plasma sheet (Gabrielse et al., 2014). Energetic particle injections, and processes to bring those particles earthward such as dipolarizing flux bundles (DFBs) and bursty bulk flows (BBFs) are all associated with substorm activity (Angelopoulos et al., 1992; Birn et al., 1998; Runov et al., 2011; Liu et al., 2013; Baker et al., 2016). If particles are injected into the inner magnetosphere, they are trapped in closed drift orbits, and they can populate the ring current, be a seed population for relativistic electrons in the radiation belt (Jaynes et al., 2015), and create anisotropies that drive wave formation meaning that an understanding of injections is required to describe a host of inner magnetospheric processes.

Although the exact details of the injection process vary in each case, the growing picture is that it starts with reconnection occurring in the tail. Then the tail magnetic field which had been stretched dipolarizes and there is a flow of particles earthward. It is thought that the electrons in this flow are accelerated primarily by betatron acceleration (Li et al., 1998; Gabrielse et al., 2016; Turner et al., 2016; Gabrielse et al., 2017; Ma et al., 2020). Ions are also accelerated at the same time, such as from interacting with dipolarization fronts (Zhou et al., 2010; Malykhin et al., 2019). A variety of phenomena can result from these flow bursts in different situations. Bursty bulk flows (BBFs) are high-speed Earthward flows in the tail that last ∼10 min but transport large amounts of energy and are associated with a dipolarization of the magnetic field (Angelopoulos et al., 1992). They can also rebound and create flows oscillating between earthward and tailward and resultant vortices as the flow brakes (Panov et al., 2010). One BBF can contain several distinct flow bursts (Angelopoulos et al., 1992; Runov et al., 2015). Observations from Cluster have shown that BBFs are very common in the plasma sheet and responsible for even more energy and mass transport than initially thought (Cao et al., 2006). Dipolarizing flux bundles (DFBs) are often observed, which are smaller flux tubes with more dipolar fields. DFBs are typically embedded in BBFs and are responsible for much of the flux transport in a BBF despite only lasting for a fraction of the time (Liu et al., 2014). Dipolarization fronts (DFs) are kinetic-scale boundaries between the earthward traveling DFB and the ambient plasma. As they travel, they deflect the plasma they are moving into and cause the tail field as a whole to dipolarize (Nakamura et al., 2002). DFs play an important role in acceleration and energy conversion. The geometry of the DF can lead to electron acceleration from either betatron or, less often, Fermi acceleration (Wu et al., 2013), and the DF has an electric field that can accelerate particles as well (Fu et al., 2012). There are also waves present, including around the lower hybrid and ion cyclotron frequencies, that can play a role in energy conversion (Huang et al., 2012; 2015). All of these phenomena described above can be present for a single event, or some of them may be observed without the others present. They also do not necessarily result in particle injection into the inner magnetosphere. Boakes et al. (2011) found that about 1/3 of substorm events had typical particle injections at GEO, about 1/3 had some sort of enhancement that did not follow the classic injection activity, and about 1/3 showed no particle enhancement. The spatial scale of injections can vary as well. Sometimes they are extremely localized and sometimes there is a more global flow and injection across several hours of MLT (Gkioulidou et al., 2015). Injections can be correlated with narrow flow channels, where the injections are highly localized either inside of these channels or on the edge them (Gabrielse et al., 2014). One proposed picture explaining the spatial difference between injections is that fast flows with small DFBs produce mesoscale injections, and as they build up, it creates a flux pile-up that leads to large-scale dipolarization and injections (Gabrielse et al., 2019). When these particles reach the inner magnetosphere, they are injected and drift around the Earth to fill the drift shell into which they are injected. The injections are generally at $>5R_E$ (Motoba et al., 2021). Although only a small percentage of flow bursts actually inject particles at GEO (Sergeev et al., 2012), it is common enough that injections occur regularly. Therefore, searching for dipolarization fronts, bursty bulk flows, and related phenomena in the tail can be a first step in finding injections in the inner magnetosphere. Injections are also limited to an energy range of a few 10s of keV to a few hundred keV, though the exact boundaries vary between injections (Reeves, 1998; Turner et al., 2017).

Injections can be classified in many ways based on observational characteristics. First is the distinction between dispersed and dispersionless injections. A dispersionless injection is observed when the satellite measures the region where particles are injected directly so injected particles of all energies arrive at the same time, while a dispersed injection is when the satellite is azimuthally removed from the acceleration site and particles with greater energy arrive at the detector earlier than less energetic particles. When particles are injected onto a closed orbit, they drift along that shell due to the $\nabla \mathbf{B}$ and curvature drifts, which are energy-dependent. Therefore, a difference between the times that particles of two different energies reach the detector means that they had to drift from their injection site to reach the detector, and the greater the time difference, the greater the distance traveled. We can use this to calculate the distance between the source of the particles and the detector. This means that if a probe is inside the boundaries of an injection, it will observe a dispersionless injection, otherwise it

will observe a dispersed injection and the greater the dispersion, the farther the observation site is from the injection site. Sometimes "drift echoes" are also visible: when an injection has drifted all the way around a complete orbit around Earth, we can observe the same injection drift past the spacecraft, now highly dispersed (Lanzerotti et al., 1967). There is also a third case of "inversely dispersed" injections, where the injection of less energetic particles arrives before the more energetic particles (Sarris et al., 1976; Sarafopoulos and Sarris, 1988; Gabrielse et al., 2012).

When observing a flow of energetic particles in the tail, there are many factors at play that can affect the injection. Gabrielse et al. (2014) found that stronger geomagnetic activity (as measured by AL index), faster flow, and stronger dipolarization were all linked to injections in the plasma sheet at higher energies as well as higher intensity injections. Turner et al. (2017) found that the strongest injections did not necessarily penetrate farther into the magnetosphere than weaker ones, which, taken with the results from Gabrielse et al. (2014), could mean that AL index flow speed, and dipolarization strength do not necessarily indicate the depth of injection penetration. Injections have been studied in detail both in the plasma sheet and the inner magnetosphere, but multipoint observations are required to study both at the same time, which greatly limits our ability to do so. In this study, we present multipoint observations from MMS and Van Allen Probes of four different events. We will present a more detailed case study of one of these events, and then discuss the evolution of the energy spectra for all four events.

2 Instruments

The Magnetospheric Multiscale Mission (MMS) was launched in 2015 and includes four spacecraft in tight formation (Burch et al., 2016). Starting with phase two of the mission in 2017, its orbit is highly elliptical with an apogee of ~25 R_E, which allows us to access data from deeper in the tail (Fuselier et al., 2016). The primary instrument we used from MMS was the Fly's Eye Energetic Particle Spectrometer (FEEPS) (Blake et al., 2016), which is part of the Energetic Particle Detector (EPD) Investigation (Mauk et al., 2016). The FEEPS instrument measures energetic particles at 25–650 keV for electrons and 45–650 keV for protons. Each spacecraft has two FEEPS units, each one consisting of 12 eyes: nine for electrons and three for protons, and each eye has 16 energy channels. To supplement the FEEPS data, we also used data from the Fast Plasma Investigation (FPI), which covers an energy range up to 30 keV (Pollock et al., 2016). Each spacecraft has four dual FPI spectrometers for electrons and four more for ions. To give context for our particle measurements, we also used data from the FIELDS suite (Torbert et al., 2016), specifically the fluxgate magnetometer (Russell et al., 2016), search coil magnetometer (Le Contel et al., 2016), and electric field double probes (Ergun et al., 2016; Lindqvist et al., 2016).

The Van Allen Probes (RBSP) were launched in 2012 and had two probes with a separation ranging from ~0.1 to 5 R_E (Mauk et al., 2012). They were in an elliptical orbit with an apogee of ~6 R_E (Kirby et al., 2012). Our primary instrument used on Van Allen Probes was the Magnetic Electron Ion Spectrometer (MagEIS) (Blake et al., 2013; Claudepierre et al., 2021). MagEIS has four spectrometers (one low energy, two medium energy, and one high energy) that cover an energy range of 20–4,800 keV for electrons as well as a proton telescope that covers a range of 55 keV–20 MeV. We also used data from the Helium, Oxygen, Proton, and Electron Mass Spectrometer (HOPE), which covers an energy range up to 50 keV (Funsten et al., 2013). Both the MagEIS and HOPE instruments are part of the Energetic Particle, Composition, and Thermal Plasma (ECT) suite (Spence et al., 2013). Van Allen Probes was deactivated in 2019, so the timespan for which data from both MMS and Van Allen Probes is available for this study is mid-2015 to mid-2019.

The GOES satellites are weather satellites in geosynchronous orbit that also include space weather instruments including the Space Environment *in Situ* Suite (SEISS). The GOES satellites are continually being replaced and improved, but in our time period, we used satellites from the GOES-N series. We used the Energetic Particle Sensor (EPS), which covers an energy range from 30 keV to several MeV for electrons and 80 keV to over 100 MeV for protons (Hanser, 2011).

3 Data

3.1 Event search

To search for an event that showed enhancements of energetic particles at both MMS and Van Allen Probes, we decided to first find events that showed a clear sign of a reconnection-related phenomenon such as DF, BBF, or plasmoid with energetic particle enhancements at MMS, then examine the Van Allen Probes data. First, we used the reports from the Scientists in the Loop (SITL) for MMS to search for events that are associated with injections, such as DFs, BBFs, DFBs, *etc.* as described above. Once we had a list of all these events at MMS, we searched through MMS burst data for events that had the greatest flux of electrons at high energies in the FEEPS instrument at and above the 272 keV channel. This was defined by the average flux at those energies during the particle energization event. Having compiled a list of the 66 most energetic events at MMS, we then studied the Van Allen Probes data for each event in the list. We were looking for electron injections that showed a clear increase in particle flux at consecutive energy channels from 33 to 54 keV (the two lowest energy channels with data) to over

100 keV in the MagEIS instrument in either probe, RBSP-A or RBSP-B, and we searched for the 30 min following the MMS observation. In order to find this, at least one of the probes has to be near apogee, because otherwise it would be too far inside the inner magnetosphere for the injections to typically penetrate. Even when at least one spacecraft was in position to potentially see an injection, we did not observe a clear injection signature with a sudden increase of at least about a half-order of magnitude at consecutive energy channels extending above 100 keV. Some events had no increase in particle flux at all and some had a very small increase in only one or two energy channels [as in e.g., Boakes et al. (2011)], but none of the 66 events in this initial search had a clear injection at Van Allen Probes. Because the goal of this search was for events for a case study, rather than setting strict definitions of an injection, we looked for particularly intense injections that could produce an illustrative case study.

Next, we took the same list of potential injection events from the SITL reports before sorting for the highest flux events, and searched for events at the time of strongest geomagnetic activity as measured by AL index. This was following the findings of Gabrielse et al. (2014) that more intense injections were correlated with |AL|, although their study was of injections in the plasma sheet, not the inner magnetosphere like we were looking for, so the correlation may or may not hold for the events we are studying. We compiled a list of events with the highest |AL|, >350 nT, and once again looked for an injection at Van Allen Probes. This time, out of 74 total events, we found one promising candidate, from 15 August 2018 at around 11:59 UT.

To find more useful events, we expanded our search at MMS beyond burst data and searched through all survey data. We restricted distance and local time to outside of 9 R_E and an MLT between 19 and five to make sure we were on the nightside and deep enough into the tail, and then looked at events that had the highest flux above the 233 keV channel, this time based on the maximum flux in that range. This gave us 42 events, and yielded another good candidate, from 22 September 2018 at around 20:10 UT. Another event, on 30 September 2016, was not itself a good event, but on inspecting the data, we found another event earlier that day around 01:09 UT that was a good candidate.

In trying to determine why so few events at MMS had corresponding inner magnetosphere injections, one hypothesis was that the most energetic particles $\nabla\mathbf{B}$ drifted out of the injection as it traveled towards the inner magnetosphere. Events with faster flows would have a stronger duskward electric field from $-\mathbf{v}\times\mathbf{B}$ with a large -x component of $\mathbf{v}$ and a +z component of $\mathbf{B}$. That would produce an $\mathbf{E}\times\mathbf{B}$ drift to oppose the $\nabla\mathbf{B}$ drift and allow particles to penetrate deeper. We still wanted the most energetic events with faster flows, but were less strict about our limits, so to search for events with faster flows, we searched for events that had a flux increase at 88.4 keV and flows in the x-y plane with $|v_{xy}| > 800$ km/s. We did this process for both burst data with the event list from the SITL reports and survey data with the same distance and MLT restrictions as before, and produced 63 events from the burst search and 49 from the survey search. From these, we produced one more candidate, from 27 August 2018 around 07:49 UT. A table containing every event studied from these searches is included in the **Supplementary Material**.

To add further evidence that there is some connection between the observation at MMS and Van Allen Probes, we looked at ground-based observations from SuperMAG magnetometers (Gjerloev, 2012). We mapped the footpoints of the fieldlines on which MMS was located using the IRBEM library (Boscher et al., 2004-2008) and the Tsyganenko 1996 magnetic field model (Tsyganenko, 1995). Then, we studied data from magnetometers close to that site for the time at which the energetic electrons are observed at MMS. For all four of these events, there was a magnetic field disturbance measured at the same time by the ground magnetometer, showing an associated signal with the event in the tail.

Although four good events out of nearly 300 examined is a very small fraction, this cannot be used to give a quantitative evaluation of how common injections are for a few reasons. First of all, there is some overlap in events between the different search methods, and the number of events quoted for each method does not account for this. Also, a lack of injection is only one of a few reasons why we might not have been able to observe one. If the Van Allen Probes are closer to perigee, then an injection would not be able to penetrate that deep even if it reaches the inner magnetosphere at a radius closer to the probes' apogee. Additionally, a few events were discarded without even using Van Allen Probes data, either because key data from one of the sources was missing, or upon closer inspection, the MMS data was not actually an injection or related process (e.g., MMS was actually measuring the ring current and already had elevated levels of energetic electrons, there was an error in the data, *etc.*). Finally, since we were only looking for clear, intense injections, there are some events that could be classified as injections under different criteria, but were not suitable for our study and therefore discarded.

3.2 Case study

On 15 August 2018, MMS was deep in the tail near its apogee, at a GSM position of (−19.2,12.5,1.6) R_E, while Van Allen Probes were also near their apogee on the nightside. The four MMS spacecraft were in a tight tetrahedral formation, with a spacecraft separation ∼10 s of km. This is the same order of magnitude as electron gyroradii for the energetic particles we are studying, so we used data from just one spacecraft, MMS-2, for this analysis.

MMS-2 was located in the premidnight sector, at a distance of 23.0 R_E and a magnetic local time of 21.8 at 12:00 UT. MMS has burst data available from 11:57:03 UT to 12:12:33 UT. This event was selected from the search of geomagnetically active times, as measured by AL index, with a predicted AL index at 11:59:23 UT of −602.0 nT as calculated by Li et al. (2007); Luo et al. (2013).

Data for this event from MMS is shown in **Figure 1**. Panel **(a)** shows the magnetic field in GSM coordinates, panel **(b)** is the spin-averaged energetic ion flux from FEEPS, panel **(c)** is the energetic electron flux from FEEPS, panel **(d)** is the electron flux from FPI, panel **(e)** is electron density, panels **(f)** and **(g)** are the electron and ion velocity, respectively, panel **(h)** is the plasma beta, and panels **(i)** and **(j)** are the magnetic and electric field power spectra. Panel **(k)** shows the energy spectra for select times. The energization is visible in panel **(c)**, the increased flux of energetic electrons from around 11:59:30 UT until around 12:02:30 UT. The FEEPS energetic ions in panel **(b)** do not have the same time-resolution because we need to use the spin-averaged data to get enough counts, but the increase in energetic ion flux is roughly at the same times as the increase in energetic electron flux. The Bz component in panel **(a)** oscillates rapidly to both positive and negative values during the energetic electron enhancements. During this same time, there is a strong tailward flow, of several hundred km/s in ions (panel **(g)**) and 1000s of km/s in the electrons [panel **(f)**]. As shown in **Supplementary Figure S1** the velocities perpendicular and parallel to the magnetic field are of the same order of magnitude, with a perpendicular electron velocity of several hundred to thousands of km/s, so the defining flow is tailward, not along the field. Plasmoids have strong tailward flows in the plasma sheet and can contain energetic electron signatures (Hones Jr et al., 1984; Imada et al., 2005). Therefore, this is likely a plasmoid being released tailward of reconnection, and there would be a corresponding flow Earthward of the reconnection site. There is some brief wave activity in the magnetic power spectrum (panel **i**) at frequencies characteristic of whistler waves during the plasmoid, though it is obscured in the electric power spectrum (panel **j**). We were especially interested in the energy spectrum of the event, so we also took the energy spectra at certain times. The spectrum we observe is not the same as the spectrum would be in the Earthward flow, but we would expect the flow Earthward of the reconnection site to be more energetic than the tailward flow (Lu et al., 2018; Runov et al., 2018), so this at least gives us a lower bound estimate of the spectrum of the Earthward flow. Following a figure in Reeves (1998), we put energy spectra at certain times below the MMS data graphs in panel **(k)**, and mark when each spectra is from with a vertical line. The first spectrum (I, in black), from 11:57:27 UT, is from before the energetic electron event began, the middle two (II, in blue, and III, in green), from 12:00:32 UT and 12:01:24 UT, are from two peaks of the energetic electron intensity, and the last one (IV, in red), from 12:02:51 UT is from after the event passed by MMS. Comparing the spectrum before the event to the spectrum at either of the two peaks, there is a significant increase in electron flux from about keV to a few hundred keV. In **Section 3.3**, we will quantify this more precisely. In the spectrum taken after the event, there is a much larger dropout of electrons of all energies in our energy range. The electron density (panel **(e)**) drops below 0.1 cm^{-3} and the plasma β (panel **(h)**) drops to around 0.01 as well, which indicates the spacecraft moving from the plasma sheet into the tail lobe, which means we do not have an exact measurement of when the event ends.

Moving into the inner magnetosphere, there is a strong signal in both Van Allen Probes spacecraft; out of the four events we studied, this had by far the strongest injection at the highest energies in the Van Allen Probes data. Both spacecraft were near their apogee, with RBSP-A at an L shell of 6.1 at 12:00 UT and RBSP-B at an L shell of 5.6. They had a small azimuthal separation, with an MLT of 0.97 for RBSP-A and 1.18 for RBSP-B. However, a dispersed injection was visible in both spacecraft, as shown in **Figure 2**. The figure shows the electron flux from the MagEIS instrument, with data from RBSP-A on the left and RBSP-B on the right. The injection was not visible in the highest energies, at and above the 749 keV channel, but arrived at about 12:00 UT in the middle energies of around 184–597 keV and about 10 min later in the lowest energy channels, 33 keV, in both spacecraft. There are also drift echoes visible starting shortly after 12:10 UT in the medium energy channels, where the electrons from the original injection have drifted an entire orbit around Earth and past the spacecraft again, this time much more dispersed. Data from the Tixie ground magnetometer, chosen because it was near the footpoint of the fieldline on which MMS was located shows a disturbance at the same time as the flow was measured in MMS (**Supplementary Figure S2**). This suggests that the event at MMS had an effect on the ground, which means that it must have traveled through the inner magnetosphere as well. Like with the MMS data, we took an energy spectrum before the injection and one at the peak of the injection. However, since this injection was dispersed, the peak occurred at a different time for every energy channel, so the time taken as the peak for each channel is marked by a diamond. The energy spectrum includes data from the high energy range of the HOPE instrument as well as all of the MagEIS data, which has a slight overlap around 20–40 keV. An empty energy channel is what creates the gap around 140 keV. Comparing the spectra of the time before the injection and the spectra of the peak of each energy channel shows that the flux increase starts at around 20 keV and continues to a few hundred keV. Again, we will quantify this later in **Section 3.3**.

The Van Allen Probes data did not show any increase in proton flux, likely because they could not penetrate as far into the inner magnetosphere as the electrons, so next we examined data from GOES. We used GOES-14 for this study, which was located at a distance of 6.611 R_E and an MLT of 16.77 at

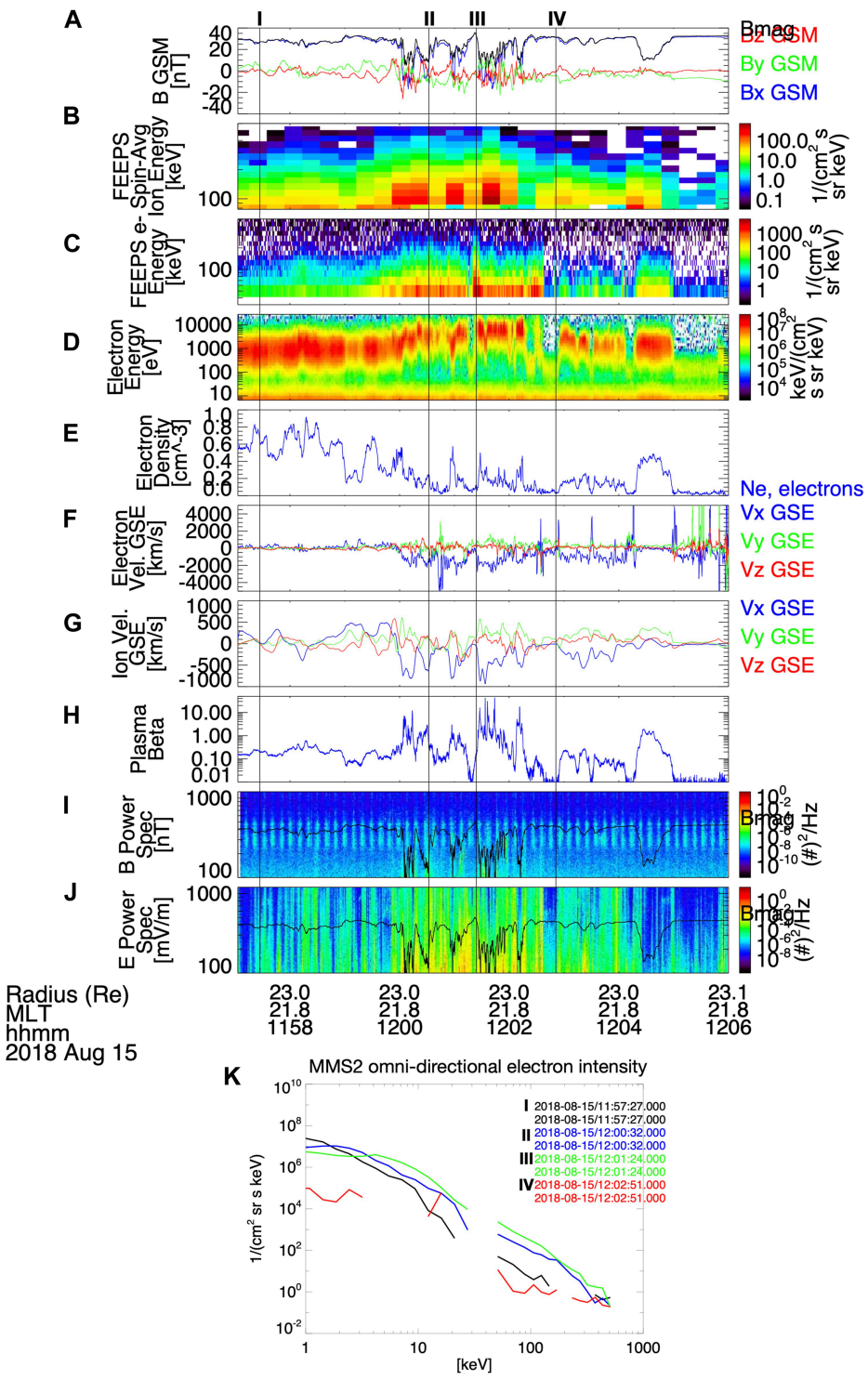

FIGURE 1
Data from MMS for the 15 August 2018 case study. **(A)** Magnetic field, **(B)** Spin-averaged FEEPS energetic ion flux, **(C)** FEEPS energetic electron flux, **(D)** FPI thermal electron flux, **(E)** Electron density, **(F)** Electron velocity, **(G)** Ion velocity, **(H)** Plasma beta, **(I)** Magnetic field power spectrum, **(J)** Electric field power spectrum. Below the MMS data, **(K)** are overlayed electron energy spectra from both the FEEPS and FPI instruments taken at a single moment at select times indicated by the vertical lines in the data: one before the energetic electron event (I), two during (II and III), and one after (IV).

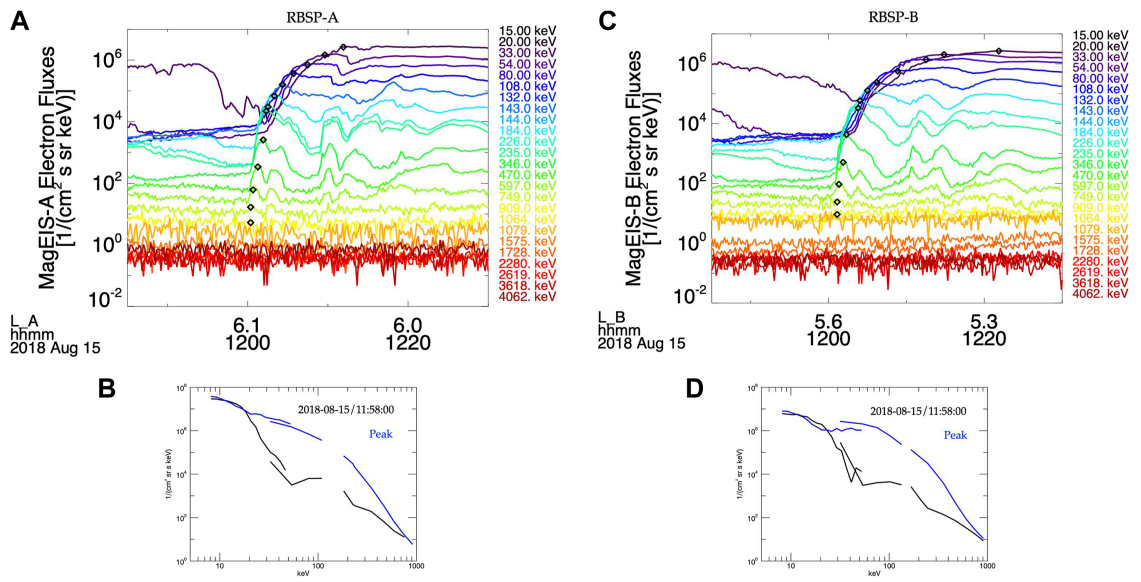

FIGURE 2
Energetic electron flux from the MagEIS instrument for the same event as **Figure 1** from RBSP-A on the left and RBSP-B on the right. The diamonds show the time of peak flux at each energy channel. Below the lineplots are energy spectra from before the injection and the peak of the injection in each energy channel.

12:00 UT. The GOES proton data shows three clear peaks in proton flux, especially in the three highest energy channels (**Figure 3**). All three are dispersed; the first one, which reaches the 575 keV channel around 12:06 UT, is significantly smaller than the other two, which reach the 575 keV channel around 12:16 UT and 12:24 UT. The later injections do not appear to be drift echoes, since the subsequent peaks are not lower and more spread out, and the amount of dispersion does not appear to be increasing.

3.3 Event comparison

3.3.1 Energy spectra changes

We analyzed the data for all four of our events like above. Although the 15 August 2018 event was the only one where we observed an injection in both Van Allen Probes spacecraft, for the other events we saw an enhancement in the energetic electrons at MMS from FEEPS, usually accompanied by some fast flow or B-field fluctuations, and then we saw an injection within a few minutes at Van Allen Probes, but only in one spacecraft since the other spacecraft was at a different radial distance. All of the injections were dispersed at Van Allen Probes. For all four events, ions were visible at MMS in either the survey or spin-averaged burst data similar to the electron signature, but there was no ion injection at Van Allen Probes. To quantify how the energy spectrum changes, we looked at the percentage of flux at each energy channel at the peak of the injection compared to before. For MMS, this was using a single time before the energetic particle enhancement and a single time at the peak of the enhancement, using the highest energy peak. The flux at the peak is averaged over 5 s and the flux before is averaged over 10 s to establish reasonable counting statistics and reduce error from random fluctuations. For Van Allen Probes, again the flux from before was a single time, but the peak was determined by the peak of each energy channel individually for the dispersed injections. The time resolution is about 11 s for MagEIS and 23 s for HOPE, so the counting statistics are sufficient to use just a single data point to make this calculation. Then, we calculated the percentage of the initial flux for each injection by taking $\left(\frac{f_p}{f_i}\right) \times 100$ for a peak flux f_p at the peak of the energization/injection event and an initial flux f_i before the event. A percentage of 100 is no change and a percentage of 1,000 is an order of magnitude flux increase. To make the error bars, we used the FESA_ERROR data product from MagEIS, which gives a percentage error (Claudepierre et al., 2015). Otherwise, for HOPE and both MMS instruments, we used the raw counts and assumed Poisson statistics, with a $\sqrt{N}$ error associated with an observation of N counts. We found the error for both the flux before the event and the flux at the peak of the event, and then propagated that through the calculation to produce error bars.

Figure 4 is the graph showing the change in energy spectra for all events at both spacecraft. Each data point is one energy channel and shows the percentage of the initial flux at the peak. The colors are consistent between the graph on the left, showing

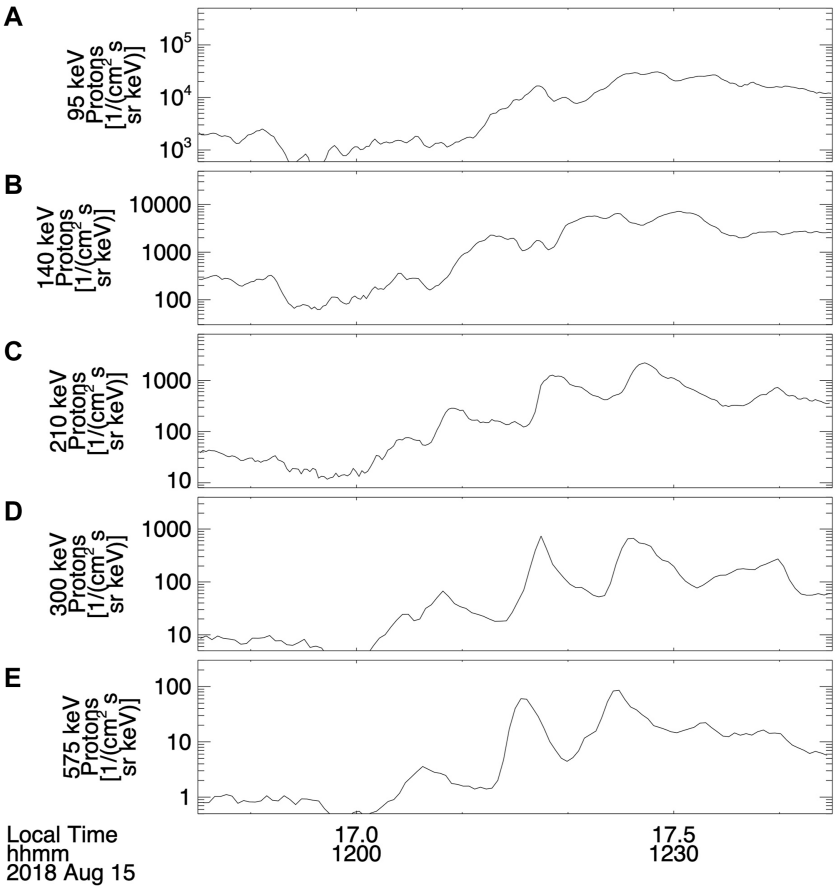

FIGURE 3
Proton flux from the GOES-14 spacecraft at **(A)** 95 keV, **(B)** 140 keV, **(C)** 210 keV, **(D)** 300 keV, and **(E)** 575 keV. There are repeated ion injections after 12:00, especially in the three highest energy channels.

the change in the spectra at MMS, and on the right, showing the change in the spectra at Van Allen Probes: the blue, green, and yellow lines show the same events on each plot, and the red and orange lines on the plot on the right are data from the two Van Allen Probes and both correspond to the red line on the left. FPI was not turned on for the 22 September 2018 event, so we only have the FEEPS data for that event, but we have coverage of the full energy range for all the other events. Comparing the two graphs, we can see that energizations extend to higher energies at MMS: there are events (the yellow line for 22 September 2018 and the blue line for 30 September 2016) that show an order of magnitude increase (percentage $>10^3$) all the way to the top of the FEEPS energy range at 508 keV. At the lower end of the energy range studied, it is less dramatic but there are still order of magnitude flux increases below 10 keV. In contrast, the energy range affected by the injection at Van Allen Probes is much more limited. Even for the most intense injection, order of magnitude flux increase is limited to around 20–400 keV. Another notable feature of these graphs is that there is no correlation between the most intense or energetic events at MMS and Van Allen Probes. While the 22 September 2018 event stands out as the most energetic event at MMS and the 15 August 2018 event is the most energetic at Van Allen Probes, neither of them are notable at the other spacecraft. This lack of comparable flux increase at the two sites suggests that the access to the inner magnetosphere is restricted for these energetic particles in a non-linear manner.

3.3.2 Injection boundaries

One other aspect of the event we studied is the spatial location and extent of the inner magnetospheric injections. Because they were all dispersed, we can use the fact that the drift is energy-dependent to map where the boundary of the injection occurred. The onset of the observed dispersed injection is when particles from the boundary of the injection site first reach the spacecraft, so we can take the particle drift velocity for each energy, knowing what time each of the energies reached the spacecraft, and track their angular drift in time

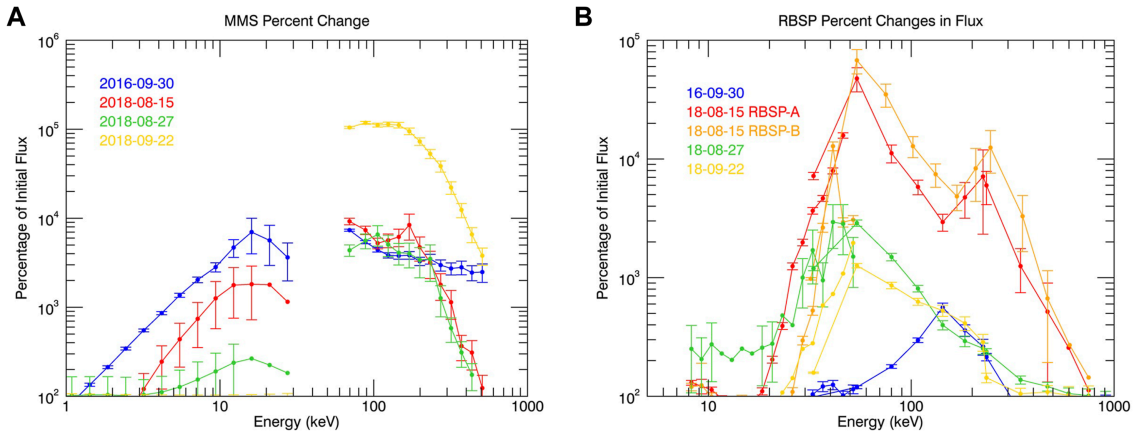

FIGURE 4
Percent change of electron flux from before the energization/injection to the peak of the energization/injection, **(A)** at MMS and **(B)** Van Allen Probes. The colors are consistent between the two, so blue (30 September 2016, 01:09 UT), green (27 August 2018, 07:49 UT), and yellow (22 September 2018, 20:10 UT) show the same events on each graph. The red event (15 August 2018, 11:59 UT) in MMS has observations from both Van Allen Probes, so both the red and orange line on the right correspond to it.

backwards to the point where all energies originated from the same spot (Reeves et al., 1990; Kanekal et al., 2016; Turner et al., 2017). Electron injections give the eastward boundary and ion injections give the westward boundary due to their drift directions. The bounce averaged drift velocity in radians/minute in a dipole field, $\langle\dot{\phi}\rangle$, is given by

$$\langle\dot{\phi}\rangle = 2\pi\frac{E}{172.4}\left(\frac{2+E}{1+E}\right)\left(\frac{m}{m_e}\right)\left(\frac{r_0}{r_E}\right)\left(\frac{F(\lambda)}{G(\lambda)}\right) \quad (1)$$

where E is the particle's kinetic energy divided by the rest mass energy, m is the particle's mass, m_e is electron mass, r_0 is the radial distance, r_E is Earth radius, and $F(\lambda)$ and $G(\lambda)$ are dimensionless functions related to the latitude that are assumed to be one since the observations are close to the equator (Lew, 1961; Kanekal et al., 2016). This assumes a dipolar field, but we acknowledge that the field is not exactly dipolar and may even be altered during the observation by dipolarization related to the injection.

We can use this to graph the trajectory in ϕ of particles of different energy, with this $\dot{\phi}$ as the slope of our graphs (**Figure 5**). The colored lines are the $\dot{\phi}$s for the different energies where there was a clear injection peak, and the dot is the location in ϕ and time where that peak was observed. Ideally, the lines would all meet in one location and that would be where the particles all were in the same location, i.e., the injection boundary, but in reality the range of where the lines for different energies intersect (the dashed lines in the figure) gives an upper and lower limit on where the boundary is in ϕ as well as when the first particles left that boundary. We take the center of that range to be our estimate for the injection boundary (the dotted lines) and the upper and lower limits give us an idea of the error in that value. From the graph, we can see that the electron boundary for all four events is premidnight, and since the ion boundary will be even earlier, this means that the injection site is contained premidnight. At Van Allen Probes, we only observe electron injections, but we can use the GOES ion injection in the 15 August 2018 event. Because electrons and ions drift in opposite direction, the lines have the opposite slope for ions as they do for electrons.

We then used this to map the location of the injection boundary in relation to the spacecraft. Going back to the 15 August 2018 event from the case study, the maps from that event in the x-y GSM plane [panel **(a,b)**] and x-z GSM plane (panel **(c)**) are shown in **Figure 6**. The map was made using the International Radiation Belt Environment Modeling (IRBEM) library (Boscher et al., 2004-2008) with the Tsyganenko 1996 magnetic field model (Tsyganenko, 1995). A few sample field lines in black are shown for reference, the green dot/field line are for MMS and the red and blue dots/field lines are for RBSP-A and RBSP-B respectively. The stars in the x-y plots are the estimated electron injection boundaries with the azimuthal angle determined by the graphs in **Figure 5** and the radial distance determined by the spacecraft location for RBSP-A (panel **(a)**) and RBSP-B (panel **(b)**) and the estimated ion boundary as determined by the same graph for GOES. Therefore, the dispersionless injection region is between the two stars and the electrons drift to the spacecraft from the boundary closer to midnight, while the ions drift from the duskward boundary. Similar maps for the other three events are included in **Supplementary Figures S3–S5**.

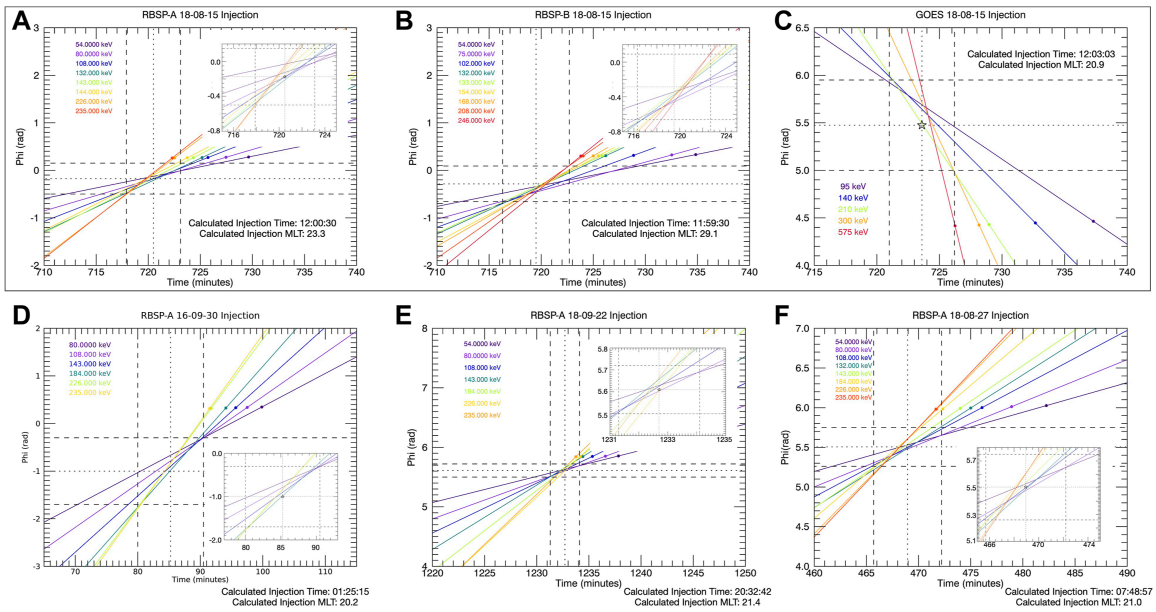

FIGURE 5
Plots to find the injection location of each dispersed electron injection at Van Allen Probes and the ion injection at GOES. The dots are the time and location of the injection at each energy, and the lines are determined by Eq. **1**. The inset of each graph shows the intersection of the lines, with the dashed lines being upper and lower bounds for the injection location, which is estimated to be the at the center of the upper and lower bounds by the star. The top row is the 15 August 2018 event at both Van Allen Probes and GOES, and the bottom row is all of the other events at just RBSP-A.

4 Discussion and conclusion

In the case study, the strong tailward flow in MMS is accompanied by a localized injection in the inner magnetosphere. We can use this to build a picture of what possibly happened. A strong, sustained tailward flow without a notable earthward flow before it does not match the damped sine wave-type flow seen by Panov et al. (2010), so this is likely not a flow rebound. Another candidate is that these energetic particles are electrons beams associated with whistler waves near the reconnection site (Wilder et al., 2016; Wang et al., 2022). However, in the pitch angle distribution of the thermal electrons, any beam-like signature is very short-lived (less than 10 s) and after the energization has already begun, so this also does not fit the case study. The more likely process is that reconnection occurs earthward of MMS and we observe the plasmoid that is being released tailward. Reconnection is known to create fast flows propagating away from the site in both directions, so there is likely a corresponding earthward flow, but there is no spacecraft in the region at the relevant time to measure it. Because energy conversion is more efficient Earthward of reconnection that tailward (Lu et al., 2018), the energetic particle population is greater Earthward of reconnection than tailward (Runov et al., 2018) and therefore our spectrum of the plasmoid at MMS is a lower bound for the spectrum of the Earthward flow. However, although energization is more efficient earthward, it still can occur tailward to an extent that energetic particles are observed in plasmoids (Hones Jr et al., 1984; Imada et al., 2005). A localized injection with a minutes-long signature like we see in Van Allen Probes is consistent with how Gabrielse et al. (2019) describe the first step of injection formation from fast earthward flows with embedded DFBs. Also an electron injection that lasts for ∼10 min or more like we see at Van Allen Probes but an ion injection that lasts for ∼5 min or less like we see at GOES is consistent with the Gabrielse et al. (2019) case study.

Because the observations at MMS and Van Allen Probes are separated so far spatially, it is hard to conclusively prove that they are related. However, at times when energetic particles are able to access the inner magnetosphere, disturbances in the tail will have effects there. Because of the particle drift, when this occurs, once particles are injected it will affect the full range of local times throughout the entire drift shell. Therefore, if the two observations are not linked, that would mean that there is an unrelated process occurring elsewhere in the tail that is causing the inner magnetospheric response, which is unlikely.

For our injection study in general, we studied four particle energization events at MMS related to reconnection-related phenomena, namely fast flows (either earthward or tailward) and dipolarization fronts, that had corresponding electron injections observed by Van Allen Probes in the inner magnetosphere

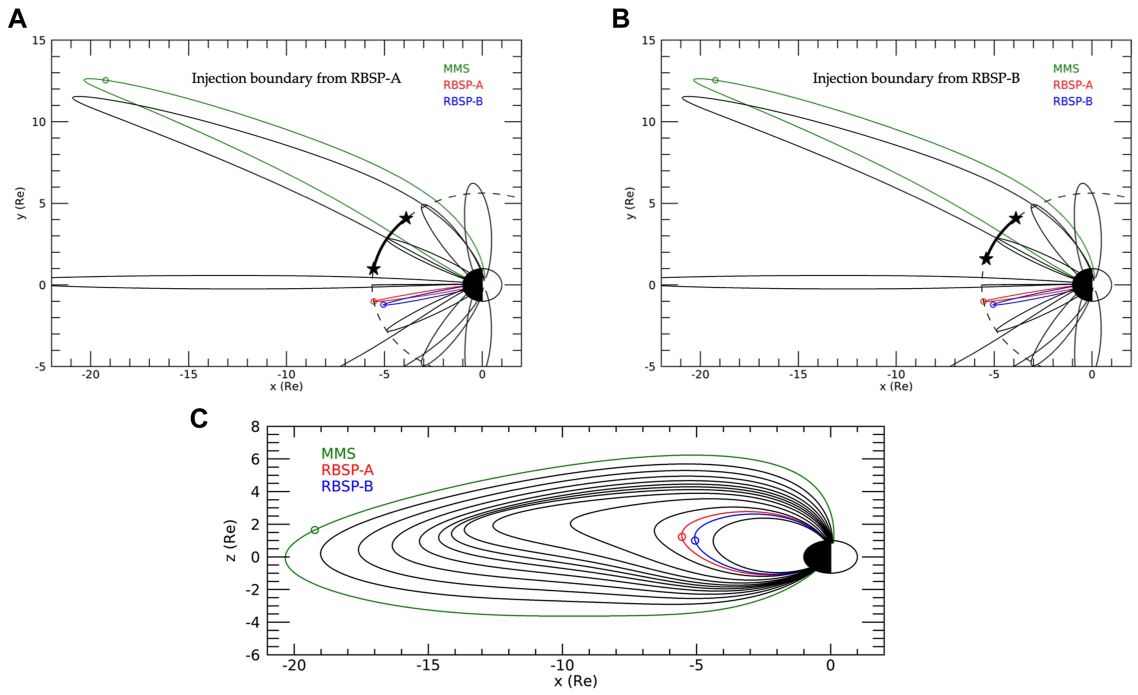

FIGURE 6
A map of the injection from the 15 August 2018 case study made in the **(A,B)** x-y and **(C)** x-z planes in GSM coordinates. The green, red, and blue circles are the locations of MMS, RBSP-A, and RBSP-B respectively at 12:00 UT. The estimated electron injection boundary as determined by **(A)** RBSP-A and **(B)** RBSP-B and ion injection boundary as determined by GOES-14 are given by the stars. The solid line connecting the two stars is an estimate for the region where the injection takes place. These were made using the IRBEM library (Boscher et al., 2004-2008) using the Tsyganenko 1996 magnetic field model (Tsyganenko, 1995).

within 30 min of the energization event at MMS. No events had corresponding ion injections observed by Van Allen Probes, although one event had a corresponding ion injection observed by GOES in GEO. This is despite the Van Allen Probe with which we observed the electron injection being located in an L-shell in the range of about 4.9–6.2, which is a region in which ion injections have been widely observed (Gkioulidou et al., 2015; Liu et al., 2016; Motoba et al., 2018) and a region in which dipolarizations have been shown to efficiently accelerate ions to energies of a few hundred keV (Ukhorskiy et al., 2017), though ion injections do not occur for every event. All of the electron injections fall mostly in the expected energy range of 10 s–100 s of keV, as in studies such as Reeves (1998). The lower energy bound for order of magnitude flux increase at MMS in one injection, 30 September 2016, drops as low as ∼4 keV, similar to the 7–9 keV range given in Turner et al. (2016). The same study also found upper energy limits ranging from 100–500 keV with repeated injections increasing the upper boundary. The most energetic injection (15 August 2018) in our study did have multiple injections over the previous few hours observed by Van Allen Probes.

The observation of all four injections occurring premidnight in the inner magnetosphere and the tail follows expected patterns: although the electron injection boundary occurs dawnward of the ion boundary, the distribution of injections is skewed duskward so the ion boundaries are strongly premidnight and the electron boundaries are only slightly more likely to be premidnight or distributed more symmetrically about midnight (Sarris et al., 1976; Gabrielse et al., 2014). Other phenomena that have been correlated with injections have also been found to be more likely to occur premidnight both in the inner magnetosphere and in the tail, such as fast flows (Raj et al., 2002; Runov et al., 2005; McPherron et al., 2011), DFBs (Liu et al., 2014), and flux ropes associated with reconnection (Imber et al., 2011).

In summary, we attempt to study events that include both particle energization in the tail at MMS and injections in the inner magnetosphere at Van Allen Probes, but it was very rare to find such events. Because particles can be injected at a range of radial distances but Van Allen Probes only reach out to L ∼6, this spacecraft configuration cannot comprehensively study all these events. We present a detailed case study of an injection that includes energetic particle enhancements, dipolarizations, and a fast tailward flow in the tail at MMS, electron injections but no ion injections in the inner magnetosphere at Van Allen Probes, and ion injections at GEO from GOES. Then we studied four

different events that had electron injections at Van Allen Probes, located premidnight, and energetic particle enhancements at MMS and found that significant flux increase at Van Allen Probes was limited to about 20–400 keV, consistent with earlier studies, while it continued higher to at least 600 keV for some events at MMS. Comparing the flux changes at MMS and Van Allen Probes, there is a lack of comparable flux increase at the two, where the flux increase by percentage is higher at MMS and the most intense injections at Van Allen Probes and MMS are different events. This suggests a non-linear mechanism limiting access of the energetic particles to the inner magnetosphere. Although it would require repeated fortuitous conjunctions and is likely not possible with data currently available, a larger statistical study of events like this could refine or generalize these findings. By observing an injection along with a related flow burst, we can learn more about the properties of injections as a whole.

Data availability statement

Publicly available datasets were analyzed in this study. This data can be found here: The MMS datasets analyzed for this study can be found in the MMS Science Data Center website: https://lasp.colorado.edu/mms/sdc/or by request for dates earlier than 1 September 2015. The Van Allen Probes datasets can found at https://rbsp-ect.newmexicoconsortium.org/data_pub/. The GOES data are available at https://satdat.ngdc.noaa.gov/sem/goes/data/.

Author contributions

SC was the primary author and researcher for this study. AJ was Ph. D. advisor for the first author and contributed to work. DT advised on data products and analysis. CG advised on analysis as well. DB and TL contributed expertise on the FEEPS instrument. BM, IC, JB, and JF gave advice on data usage.

Funding

This work was supported by funding from the MMS mission, under NASA contract NNG04EB99C and NASA grant 80NSSC20K1790.

Acknowledgments

We acknowledge the superMAG collaboration for the use of their data (Gjerloev, 2012).

Conflict of interest

The authors declare that the research was conducted in the absence of any commercial or financial relationships that could be construed as a potential conflict of interest.

Publisher's note

All claims expressed in this article are solely those of the authors and do not necessarily represent those of their affiliated organizations, or those of the publisher, the editors and the reviewers. Any product that may be evaluated in this article, or claim that may be made by its manufacturer, is not guaranteed or endorsed by the publisher.

Supplementary material

The Supplementary Material for this article can be found online at: https://www.frontiersin.org/articles/10.3389/fspas.2022.1033546/full#supplementary-material

References

Angelopoulos, V., Baumjohann, W., Kennel, C., Coroniti, F. V., Kivelson, M., Pellat, R., et al. (1992). Bursty bulk flows in the inner central plasma sheet. *J. Geophys. Res. Space Phys.* 97, 4027–4039. doi:10.1029/91ja02701

Arnoldy, R. L., and Chan, K. (1969). Particle substorms observed at the geostationary orbit. *J. Geophys. Res.* 74, 5019–5028. doi:10.1029/ja074i021p05019

Baker, D., Jaynes, A., Turner, D., Nakamura, R., Schmid, D., Mauk, B., et al. (2016). A telescopic and microscopic examination of acceleration in the june 2015 geomagnetic storm: Magnetospheric multiscale and van allen probes study of substorm particle injection. *Geophys. Res. Lett.* 43, 6051–6059. doi:10.1002/2016gl069643

Birn, J., Thomsen, M., Borovsky, J., Reeves, G., McComas, D., Belian, R., et al. (1998). Substorm electron injections: Geosynchronous observations and test particle simulations. *J. Geophys. Res. Space Phys.* 103, 9235–9248. doi:10.1029/97ja02635

Blake, J., Carranza, P., Claudepierre, S., Clemmons, J., Crain, W., Dotan, Y., et al. (2013). "The magnetic electron ion spectrometer (mageis) instruments aboard the radiation belt storm probes (rbsp) spacecraft," in *The van Allen probes mission* (Springer), 383–421.

Blake, J., Mauk, B., Baker, D., Carranza, P., Clemmons, J., Craft, J., et al. (2016). The fly's eye energetic particle spectrometer (feeps) sensors for the magnetospheric multiscale (mms) mission. *Space Sci. Rev.* 199, 309–329. doi:10.1007/s11214-015-0163-x

Boakes, P., Milan, S., Abel, G. A., Freeman, M. P., Chisham, G., and Hubert, B. (2011). A superposed epoch investigation of the relation between magnetospheric

solar wind driving and substorm dynamics with geosynchronous particle injection signatures. *J. Geophys. Res. Space Phys.* 116. doi:10.1029/2010ja016007

Boscher, D., Bourdarie, S., O'Brien, P., and Guild, T. (2004-2008). *IRBEM library V4.3*.

Burch, J., Moore, T., Torbert, R., and Giles, B. (2016). Magnetospheric multiscale overview and science objectives. *Space Sci. Rev.* 199, 5–21. doi:10.1007/s11214-015-0164-9

Cao, J., Ma, Y., Parks, G., Reme, H., Dandouras, I., Nakamura, R., et al. (2006). Joint observations by cluster satellites of bursty bulk flows in the magnetotail. *J. Geophys. Res. Space Phys.* 111, A04206. doi:10.1029/2005ja011322

Claudepierre, S., O'Brien, T., Blake, J., Fennell, J., Roeder, J., Clemmons, J., et al. (2015). A background correction algorithm for van allen probes mageis electron flux measurements. *J. Geophys. Res. Space Phys.* 120, 5703–5727. doi:10.1002/2015ja021171

Claudepierre, S., Blake, J. B., Boyd, A., Clemmons, J., Fennell, J., Gabrielse, C., et al. (2021). The magnetic electron ion spectrometer: A review of on-orbit sensor performance, data, operations, and science. *Space Sci. Rev.* 217, 80–67. doi:10.1007/s11214-021-00855-2

Ergun, R., Tucker, S., Westfall, J., Goodrich, K., Malaspina, D., Summers, D., et al. (2016). The axial double probe and fields signal processing for the mms mission. *Space Sci. Rev.* 199, 167–188. doi:10.1007/s11214-014-0115-x

Fu, H. S., Khotyaintsev, Y. V., Vaivads, A., André, M., and Huang, S. (2012). Electric structure of dipolarization front at sub-proton scale. *Geophys. Res. Lett.* 39. doi:10.1029/2012gl051274

Funsten, H., Skoug, R., Guthrie, A., MacDonald, E., Baldonado, J., Harper, R., et al. (2013). "Helium, oxygen, proton, and electron (hope) mass spectrometer for the radiation belt storm probes mission," in *The van allen probes mission* (Springer), 423–484.

Fuselier, S., Lewis, W., Schiff, C., Ergun, R., Burch, J., Petrinec, S., et al. (2016). Magnetospheric multiscale science mission profile and operations. *Space Sci. Rev.* 199, 77–103. doi:10.1007/s11214-014-0087-x

Gabrielse, C., Angelopoulos, V., Runov, A., and Turner, D. (2012). The effects of transient, localized electric fields on equatorial electron acceleration and transport toward the inner magnetosphere. *J. Geophys. Res. Space Phys.* 117. doi:10.1029/2012ja017873

Gabrielse, C., Angelopoulos, V., Runov, A., and Turner, D. L. (2014). Statistical characteristics of particle injections throughout the equatorial magnetotail. *J. Geophys. Res. Space Phys.* 119, 2512–2535. doi:10.1002/2013ja019638

Gabrielse, C., Harris, C., Angelopoulos, V., Artemyev, A., and Runov, A. (2016). The role of localized inductive electric fields in electron injections around dipolarizing flux bundles. *J. Geophys. Res. Space Phys.* 121, 9560–9585. doi:10.1002/2016ja023061

Gabrielse, C., Angelopoulos, V., Harris, C., Artemyev, A., Kepko, L., and Runov, A. (2017). Extensive electron transport and energization via multiple, localized dipolarizing flux bundles. *J. Geophys. Res. Space Phys.* 122, 5059–5076. doi:10.1002/2017ja023981

Gabrielse, C., Spanswick, E., Artemyev, A., Nishimura, Y., Runov, A., Lyons, L., et al. (2019). Utilizing the heliophysics/geospace system observatory to understand particle injections: Their scale sizes and propagation directions. *J. Geophys. Res. Space Phys.* 124, 5584–5609. doi:10.1029/2018ja025588

Gjerloev, J. (2012). The supermag data processing technique. *J. Geophys. Res. Space Phys.* 117, 1924–1938. doi:10.1029/2012ja017683

Gkioulidou, M., Ohtani, S., Mitchell, D., Ukhorskiy, A., Reeves, G., Turner, D., et al. (2015). Spatial structure and temporal evolution of energetic particle injections in the inner magnetosphere during the 14 july 2013 substorm event. *J. Geophys. Res. Space Phys.* 120, 1924–1938. doi:10.1002/2014ja020872

Hanser, F. (2011). *Eps/hepad calibration and data handbook (tech. rep. goesn-eng-048d)*. Carlisle, MA: Assurance Technology Corporation.

Hones, E.Jr, Birn, J., Baker, D., Bame, S., Feldman, W., McComas, D., et al. (1984). Detailed examination of a plasmoid in the distant magnetotail with isee 3. *Geophys. Res. Lett.* 11, 1046–1049. doi:10.1029/gl011i010p01046

Huang, S., Zhou, M., Deng, X., Yuan, Z., Pang, Y., Wei, Q., et al. (2012). Kinetic structure and wave properties associated with sharp dipolarization front observed by cluster. *Ann. Geophys. Copernic. GmbH)* 30, 97–107. doi:10.5194/angeo-30-97-2012

Huang, S., Fu, H., Yuan, Z., Zhou, M., Fu, S., Deng, X., et al. (2015). Electromagnetic energy conversion at dipolarization fronts: Multispacecraft results. *J. Geophys. Res. Space Phys.* 120, 4496–4502. doi:10.1002/2015ja021083

Imada, S., Hoshino, M., and Mukai, T. (2005). Average profiles of energetic and thermal electrons in the magnetotail reconnection regions. *Geophys. Res. Lett.* 32, L09101. doi:10.1029/2005gl022594

Imber, S., Slavin, J., Auster, H., and Angelopoulos, V. (2011). A themis survey of flux ropes and traveling compression regions: Location of the near-earth reconnection site during solar minimum. *J. Geophys. Res. Space Phys.* 116. doi:10.1029/2010ja016026

Jaynes, A. N., Baker, D. N., Singer, H. J., Rodriguez, J. V., Loto'aniu, T., Ali, A., et al. (2015). Source and seed populations for relativistic electrons: Their roles in radiation belt changes. *J. Geophys. Res. Space Phys.* 120, 7240–7254. doi:10.1002/2015ja021234

Kanekal, S., Baker, D., Fennell, J., Jones, A., Schiller, Q., Richardson, I., et al. (2016). Prompt acceleration of magnetospheric electrons to ultrarelativistic energies by the 17 march 2015 interplanetary shock. *J. Geophys. Res. Space Phys.* 121, 7622–7635. doi:10.1002/2016ja022596

Kirby, K., Artis, D., Bushman, S., Butler, M., Conde, R., Cooper, S., et al. (2012). "Radiation belt storm probes—Observatory and environments," in *The van allen probes mission* (Springer), 59–125.

Lanzerotti, L., Roberts, C., and Brown, W. (1967). Temporal variations in the electron flux at synchronous altitudes. *J. Geophys. Res.* 72, 5893–5902. doi:10.1029/jz072i023p05893

Le Contel, O., Leroy, P., Roux, A., Coillot, C., Alison, D., Bouabdellah, A., et al. (2016). The search-coil magnetometer for mms. *Space Sci. Rev.* 199, 257–282. doi:10.1007/s11214-014-0096-9

Lew, J. S. (1961). Drift rate in a dipole field. *J. Geophys. Res.* 66, 2681–2685. doi:10.1029/jz066i009p02681

Li, X., Baker, D., Temerin, M., Reeves, G., and Belian, R. (1998). Simulation of dispersionless injections and drift echoes of energetic electrons associated with substorms. *Geophys. Res. Lett.* 25, 3763–3766. doi:10.1029/1998gl900001

Li, X., Oh, K. S., and Temerin, M. (2007). Prediction of the al index using solar wind parameters. *J. Geophys. Res. Space Phys.* 112. doi:10.1029/2006ja011918

Lindqvist, P.-A., Olsson, G., Torbert, R., King, B., Granoff, M., Rau, D., et al. (2016). The spin-plane double probe electric field instrument for mms. *Space Sci. Rev.* 199, 137–165. doi:10.1007/s11214-014-0116-9

Liu, J., Angelopoulos, V., Runov, A., and Zhou, X.-Z. (2013). On the current sheets surrounding dipolarizing flux bundles in the magnetotail: The case for wedgelets. *J. Geophys. Res. Space Phys.* 118, 2000–2020. doi:10.1002/jgra.50092

Liu, J., Angelopoulos, V., Zhou, X.-Z., and Runov, A. (2014). Magnetic flux transport by dipolarizing flux bundles. *J. Geophys. Res. Space Phys.* 119, 909–926. doi:10.1002/2013ja019395

Liu, J., Angelopoulos, V., Zhang, X.-J., Turner, D. L., Gabrielse, C., Runov, A., et al. (2016). Dipolarizing flux bundles in the cis-geosynchronous magnetosphere: Relationship between electric fields and energetic particle injections. *J. Geophys. Res. Space Phys.* 121, 1362–1376. doi:10.1002/2015ja021691

Lu, S., Pritchett, P., Angelopoulos, V., and Artemyev, A. (2018). Magnetic reconnection in earth's magnetotail: Energy conversion and its earthward–tailward asymmetry. *Phys. Plasmas* 25, 012905. doi:10.1063/1.5016435

Luo, B., Li, X., Temerin, M., and Liu, S. (2013). Prediction of the au, al, and ae indices using solar wind parameters. *J. Geophys. Res. Space Phys.* 118, 7683–7694. doi:10.1002/2013ja019188

Ma, W., Zhou, M., Zhong, Z., and Deng, X. (2020). Electron acceleration rate at dipolarization fronts. *Astrophys. J.* 903, 84. doi:10.3847/1538-4357/abb8cc

Malykhin, A. Y., Grigorenko, E. E., Kronberg, E. A., Daly, P. W., and Kozak, L. V. (2019). Acceleration of protons and heavy ions to suprathermal energies during dipolarizations in the near-earth magnetotail. *Ann. Geophys. Copernic. GmbH)* 37, 549–559. doi:10.5194/angeo-37-549-2019

Mauk, B., Fox, N. J., Kanekal, S., Kessel, R., Sibeck, D., and Ukhorskiy, a. A. (2012). "Science objectives and rationale for the radiation belt storm probes mission," in *The van allen probes mission* (Springer), 3–27.

Mauk, B., Blake, J., Baker, D., Clemmons, J., Reeves, G., Spence, H. E., et al. (2016). The energetic particle detector (epd) investigation and the energetic ion spectrometer (eis) for the magnetospheric multiscale (mms) mission. *Space Sci. Rev.* 199, 471–514. doi:10.1007/s11214-014-0055-5

McPherron, R., Hsu, T.-S., Kissinger, J., Chu, X., and Angelopoulos, V. (2011). Characteristics of plasma flows at the inner edge of the plasma sheet. *J. Geophys. Res. Space Phys.* 116. doi:10.1029/2010ja015923

Motoba, T., Ohtani, S., Gkioulidou, M., Ukhorskiy, A., Mitchell, D., Takahashi, K., et al. (2018). Response of different ion species to local magnetic dipolarization inside geosynchronous orbit. *J. Geophys. Res. Space Phys.* 123, 5420–5434. doi:10.1029/2018ja025557

Motoba, T., Ohtani, S., Gkioulidou, M., Ukhorskiy, A., Lanzerotti, L. J., and Claudepierre, S. G. (2021). Dynamic properties of particle injections inside geosynchronous orbit: A multisatellite case study. *J. Geophys. Res. Space Phys.* 126, e2020JA028215. doi:10.1029/2020JA028215

Nakamura, R., Baumjohann, W., Klecker, B., Bogdanova, Y., Balogh, A., Rème, H., et al. (2002). Motion of the dipolarization front during a flow burst event observed by cluster. *Geophys. Res. Lett.* 29, 3-1–3-4. doi:10.1029/2002gl015763

Panov, E., Nakamura, R., Baumjohann, W., Angelopoulos, V., Petrukovich, A., Retinò, A., et al. (2010). Multiple overshoot and rebound of a bursty bulk flow. *Geophys. Res. Lett.* 37. doi:10.1029/2009gl041971

Pollock, C., Moore, T., Jacques, A., Burch, J., Gliese, U., Saito, Y., et al. (2016). Fast plasma investigation for magnetospheric multiscale. *Space Sci. Rev.* 199, 331–406.

Raj, A., Phan, T., Lin, R. P., and Angelopoulos, V. (2002). Wind survey of high-speed bulk flows and field-aligned beams in the near-earth plasma sheet. *J. Geophys. Res. Space Phys.* 107, SMP 3-1–SMP 3-17. doi:10.1029/2001ja007547

Reeves, G., Fritz, T., Cayton, T., and Belian, R. (1990). Multi-satellite measurements of the substorm injection region. *Geophys. Res. Lett.* 17, 2015–2018. doi:10.1029/gl017i011p02015

Reeves, G. D. (1998). *New perspectives on substorm injections*. Tech. rep. Los Alamos, NM (United States): Los Alamos National Lab.

Runov, A., Sergeev, V., Nakamura, R., Baumjohann, W., Zhang, T., Asano, Y., et al. (2005). Reconstruction of the magnetotail current sheet structure using multi-point cluster measurements. *Planet. Space Sci.* 53, 237–243. doi:10.1016/j.pss.2004.09.049

Runov, A., Angelopoulos, V., Zhou, X.-Z., Zhang, X.-J., Li, S., Plaschke, F., et al. (2011). A themis multicase study of dipolarization fronts in the magnetotail plasma sheet. *J. Geophys. Res. Space Phys.* 116. doi:10.1029/2010ja016316

Runov, A., Angelopoulos, V., Gabrielse, C., Liu, J., Turner, D., and Zhou, X.-Z. (2015). Average thermodynamic and spectral properties of plasma in and around dipolarizing flux bundles. *J. Geophys. Res. Space Phys.* 120, 4369–4383. doi:10.1002/2015ja021166

Runov, A., Angelopoulos, V., Artemyev, A., Lu, S., and Zhou, X.-Z. (2018). Near-earth reconnection ejecta at lunar distances. *J. Geophys. Res. Space Phys.* 123, 2736–2744. doi:10.1002/2017ja025079

Russell, C., Anderson, B., Baumjohann, W., Bromund, K., Dearborn, D., Fischer, D., et al. (2016). The magnetospheric multiscale magnetometers. *Space Sci. Rev.* 199, 189–256. doi:10.1007/s11214-014-0057-3

Sarafopoulos, D., and Sarris, E. (1988). Inverse velocity dispersion of energetic particle bursts inside the plasma sheet. *Planet. space Sci.* 36, 1181–1199. doi:10.1016/0032-0633(88)90072-4

Sarris, E., Krimigis, S., and Armstrong, T. (1976). Observations of magnetospheric bursts of high-energy protons and electrons at $\sim 35 R_E$ with Imp 7. *J. Geophys. Res.* 81, 2341–2355. doi:10.1029/ja081i013p02341

Sergeev, V., Chernyaev, I., Dubyagin, S., Miyashita, Y., Angelopoulos, V., Boakes, P., et al. (2012). Energetic particle injections to geostationary orbit: Relationship to flow bursts and magnetospheric state. *J. Geophys. Res. Space Phys.* 117. doi:10.1029/2012ja017773

Spence, H. E., Reeves, G., Baker, D., Blake, J., Bolton, M., Bourdarie, S., et al. (2013). Science goals and overview of the radiation belt storm probes (rbsp) energetic particle, composition, and thermal plasma (ect) suite on nasa's van allen probes mission. *Space Sci. Rev.* 179, 311–336. doi:10.1007/s11214-013-0007-5

Torbert, R., Russell, C., Magnes, W., Ergun, R., Lindqvist, P.-A., LeContel, O., et al. (2016). The fields instrument suite on mms: Scientific objectives, measurements, and data products. *Space Sci. Rev.* 199, 105–135. doi:10.1007/s11214-014-0109-8

Tsyganenko, N. (1995). Modeling the earth's magnetospheric magnetic field confined within a realistic magnetopause. *J. Geophys. Res. Space Phys.* 100, 5599–5612. doi:10.1029/94ja03193

Turner, D. L., Fennell, J., Blake, J., Clemmons, J., Mauk, B., Cohen, I., et al. (2016). Energy limits of electron acceleration in the plasma sheet during substorms: A case study with the magnetospheric multiscale (mms) mission. *Geophys. Res. Lett.* 43, 7785–7794. doi:10.1002/2016gl069691

Turner, D. L., Fennell, J., Blake, J., Claudepierre, S., Clemmons, J., Jaynes, A., et al. (2017). Multipoint observations of energetic particle injections and substorm activity during a conjunction between magnetospheric multiscale (mms) and van allen probes. *J. Geophys. Res. Space Phys.* 122, 11–481. doi:10.1002/2017ja024554

Ukhorskiy, A., Sitnov, M., Merkin, V., Gkioulidou, M., and Mitchell, D. (2017). Ion acceleration at dipolarization fronts in the inner magnetosphere. *J. Geophys. Res. Space Phys.* 122, 3040–3054. doi:10.1002/2016ja023304

Wang, S., Bessho, N., Graham, D. B., Le Contel, O., Wilder, F. D., Khotyaintsev, Y. V., et al. (2022). Whistler waves associated with electron beams in magnetopause reconnection diffusion regions. *J. Geophys. Res. Space Phys.* 127, e2022JA030882. doi:10.1029/2022ja030882

Wilder, F., Ergun, R., Goodrich, K., Goldman, M., Newman, D., Malaspina, D., et al. (2016). Observations of whistler mode waves with nonlinear parallel electric fields near the dayside magnetic reconnection separatrix by the magnetospheric multiscale mission. *Geophys. Res. Lett.* 43, 5909–5917. doi:10.1002/2016gl069473

Wu, M., Lu, Q., Volwerk, M., Voeroes, Z., Zhang, T., Shan, L., et al. (2013). A statistical study of electron acceleration behind the dipolarization fronts in the magnetotail. *J. Geophys. Res. Space Phys.* 118, 4804–4810. doi:10.1002/jgra.50456

Zhou, X.-Z., Angelopoulos, V., Sergeev, V., and Runov, A. (2010). Accelerated ions ahead of earthward propagating dipolarization fronts. *J. Geophys. Res. Space Phys.* 115. doi:10.1029/2010ja015481